Thermodynamics and Structure of Single- and Two-Phase Yttria−Alumina Glasses

Jean A. Tangeman,*,† Brian L. Phillips,‡ Paul C. Nordine,† and J. K. Richard Weber†

Containerless Research, Inc., 906 University Place, Evanston, Illinois 60201, and State University of New York at Stony Brook, Department of Geosciences, Stony Brook, New York 11794-2100

Received: December 19, 2002; In Final Form: December 8, 2003

Yttria−alumina (YA) glasses containing 59.8−75.6 mol % Al_2O_3 were synthesized in the form of 1−3.5 mm diameter spheroids using containerless techniques. The glasses formed at cooling rates ranging from <70 K/s at compositions near 72 mol % Al_2O_3 and up to 300 K/s at the ends of the composition range. Samples with compositions from 59.8 to ∼69.0 mol % Al_2O_3 contained two glass phases, with an immiscible droplet (∼1−20 μm diameter) phase in the matrix glass. A single glass phase was formed at greater alumina concentrations. Glasses near the alumina- and yttria-rich ends of the compositional suite also contained ∼5−20% and 1−2% crystals, respectively. Heat capacities (C_P) of the glasses and supercooled liquids, glass transition temperatures (T_g), configurational heat capacities at T_g ($\Delta C_P(T_g)$), and glass structures were investigated using differential scanning calorimetry (DSC) and ^{27}Al MAS NMR spectroscopy. The T_g increases slightly with alumina content, from 1146 to 1156 K. The C_p increases ∼60% at T_g to form a highly fragile supercooled liquid. The concentrations of 4-, 5-, and 6-coordinate Al^{3+} ions in a single-phase glass with 71.5 mol % Al_2O_3 (Y71.5A) are ∼68% ± 4, 27% ± 3, and 6% ± 2, respectively. A minimum 6- and maximum 5-coordinate Al^{3+} concentration occurs near the Y71.5A composition, which is one of the best glass formers. In the context of the structural and thermodynamic properties reported herein, the formation mechanism and coordination of polyamorphic YA glasses are discussed.

1. Introduction

The yttria−alumina (Y_2O_3−Al_2O_3; YA) pseudo-binary system displays a variety of nonequilibrium phenomena, including glass formation, metastable crystallization,[1] and polyamorphism in the undercooled liquid.[2] Coutures et al.[3] first investigated undercooled yttrium aluminum garnet (YAG, $Y_3Al_5O_{12}$)-composition melts under containerless conditions. They reported glass formation, spontaneous crystallization of YAG, or spontaneous crystallization to form a mixture of alumina (α-Al_2O_3) and $YAlO_3$ (YAP), depending on the cooling rate and process conditions. Nagashio et al.[4] and Weber et al.[5] showed that the critical cooling rate for glass formation from the YAG composition is approximately 150 K/s under containerless conditions. Glass can be formed over the composition range from about 58−77 mol % aluminum oxide[5] by increasing the cooling rate of the liquid under containerless conditions.

Aasland and McMillan[2] observed evidence of a liquid−liquid-phase transition in undercooled YA melts containing 68−76 mol % alumina. Samples formed by melting powdered oxides on an electrically heated iridium filament contained two glasses with essentially identical composition (demonstrated for a sample containing 71 mol % alumina, the balance yttria) but different densities. Weber et al.[5] confirmed this result for a YA glass with 67.5 mol % alumina.

Florian et al.[6] showed by ^{27}Al NMR spectroscopy that glass of the YAG composition contains Al^{3+} in 4-, 5-, and 6-coordination environments. In addition, evidence for two distinct 5-coordinate Al^{3+} species was presented, suggesting that differentiation of the Al environment may play a role in formation of the two-phase, polyamorphic glass. Using triple quantum ^{27}Al MAS NMR spectroscopy, Wilding et al.[7] also showed that three structural units (AlO_4, AlO_5, and AlO_6) are present in both single- and two-phase alumina-yttria glasses, as well as a heat treated single-phase glass, and that the relative proportions of these structural units appeared to be essentially the same for the three different glasses within resolution of the measurements. They further reported that accompanying the liquid−liquid transition in Y_2O_3−Al_2O_3 liquids is a decrease in the degree of distortion of the Al−O units and an increase in the midrange order. X-ray scattering results for a liquid of YAG composition[8] yield Al−O coordination values in the range from 3.6 to 5.1 ± 0.5. Al−O peaks in the radial distribution functions are at ∼1.80 Å for both the glass[9] and liquid,[8] consistent with ∼4-coordinate Al−O bonding. Neutron diffraction results[9,10] yield an Al−O coordination of ∼4.2 and ∼4.4 for glasses containing 75 and 80 mol % alumina, respectively.

Data on the rheological properties of YA liquids include the results of Fratello and Brandle,[11] who showed that molten YAG (62.5 mol % alumina) has a small and weakly temperature-dependent viscosity at 2240−2340 K. Weber et al.[12] showed that the viscosity of the undercooled liquid is sufficient to permit glass fiber pulling in the temperature range, 1600−1650 K, consistent with a non-Arrhenian temperature dependence of viscosity, i.e. a fragile liquid.

Lin et al.[13] measured the devitrification enthalpy of YAG-composition glass, which is 13.8 kJ/g atom, compared with 21 kJ/g atom for the fusion enthalpy.[1] Combined with data on the glass transition temperature,[14] and the fusion temperature,[11]

* To whom correspondence should be addressed. Phone: (847) 467-2678. Fax: (847) 467-2679. E-mail: tangeman@containerless.com.
† Containerless Research, Inc.
‡ State University of New York at Stony Brook.

10.1021/jp027779e CCC: $27.50
Published on Web 07/22/2004

TABLE 1: Measured Compositions of Alumina−Yttria Glasses

sample	Al_2O_3 (mol %)	Al_2O_3 (wt %)	Y_2O_3 (wt %)	total (wt %)	phases	cooling rates (K/s)
Y76A	75.63	58.30 (0.26)	41.51 (0.28)	99.81	[g1],[x]	250−330
Y75A	75.43	57.98 (0.54)	41.82 (0.49)	99.80	[g1],[x]	230−310
Y74A	74.18	55.81 (0.45)	43.03 (0.21)	98.84	[g1],[x]	100−180
Y73.5A	73.14	54.47 (1.06)	44.30 (0.79)	98.77	[g1],[x] or [g1]	60−140
Y72.5A	72.46	54.14 (1.07)	45.57 (0.81)	99.71	[g1]	60−140
Y71.5A	71.42	52.40 (0.39)	46.44 (0.42)	98.84	[g1]	50−120
Y69A	68.99	50.02 (0.25)	49.79 (0.48)	99.81	[g1],[g2] or [g1]	80−140
Y67A	67.62	48.05 (0.52)	50.96 (0.46)	99.01	[g1],[g2]	90−150
Y65A	64.49	44.47 (0.74)	54.22 (0.47)	98.69	[g1],[g2]	100−200
Y65A matrix	64.53	54.35 (0.43)	44.65 (0.34)	99.00	[g1]	
Y65A spherule	65.28	54.18 (0.29)	45.99 (0.22)	100.17	[g2]	
Y62.5A	62.10	42.17 (0.31)	57.01 (0.25)	99.18	[g1],[g2],[x]	180−240
Y60A	59.79	39.80 (0.50)	59.29 (0.28)	99.09	[g1],[g2],[x]	230−300

these results show that the average heat capacity of undercooled YAG-composition liquid is approximately 6.6 J/g atom greater than for the crystalline solid, and provide further evidence of the fragility of YAG-composition liquid.

The observation of polyamorphism in YA glasses/liquids and the potential utility of rare-earth and yttria containing alumina-based glasses as hosts for laser active ions render these glasses excellent candidates for both phenomenological studies and applied materials research. Currently, relatively little thermodynamic and structural data on vitreous aluminates are available, because rare-earth aluminate materials typically have very high melting temperatures and tend to crystallize during quenching.[12] By conventional glass-forming techniques, these materials are extremely difficult to vitrify. The purpose of the current investigation was first to use containerless techniques to synthesize a suite of glasses over a relatively large compositional range in the alumina−yttria system. Following synthesis, high-field NMR spectroscopy and differential scanning calorimetry were used to discern structural and thermodynamic differences between the single- and two-phase glasses in the system.

2. Experimental Procedures

2.1. Sample Composition and Synthesis. The eleven YA compositions given in Table 1 were prepared in 5 g batches by mixing 99.99% pure Y_2O_3 and Al_2O_3 powders (Cerac, Inc., Milwaukee, WI). Weighed powders were homogenized in a ball mill and fused in a laser hearth[15] into a crystalline boule. The resulting boule was ground to a powder, remelted in the hearth in the same manner, and then crushed into pieces 2−3.5 mm in diameter. The 2−3.5 mm diameter samples were levitated in pure argon gas in a conical nozzle levitator (CNL)[5] and were heated and melted with a partially focused continuous-wave CO_2 laser. The liquid was superheated by ∼50 K to ensure complete melting, held for ∼10 s, and then cooled by blocking the heating laser beam. Sample temperatures were measured at a rate of 30 Hz with an automatic optical pyrometer (effective wavelength ∼650 nm) and the temperature data were acquired by computer.[5] Larger samples cooled more slowly and, in some cases, crystallized spontaneously. Smaller samples cooled faster and formed glass. Crystallization was readily detected by the rapid temperature rise (recalescence) when the heat of fusion was released, observed as a "spike" in the pyrometer output. Samples that formed glass, or contained only a trace of crystals, showed no evidence of spontaneous heat release and were saved for analysis.

About 2−3 g of glass spheroids were made from each composition. The glass samples were first examined for evidence of phase separation using an optical microscope and 100× magnification. In addition, backscattered electron (BSE) images were subsequently acquired with a scanning electron microscope on polished cross sections of the samples. Chemical compositions of all of the glasses were analyzed using a Cameca SX-50 electron microprobe. Quantitative, wavelength-dispersive analyses were performed at 20 keV with a beam current of 10 nA using an approximately 1 μm diameter electron beam. Measurements were obtained on three glass spheroids for each composition, at several points across the diameter of the polished and carbon coated surfaces. Analyses using the above instrument, of both the droplet phase and the matrix phase, were determined for Y65A glass. Single-crystal yttrium aluminum garnet (YAG: $Y_3Al_5O_{12}$) was used as the standard for Y_2O_3 and Al_2O_3, in conjunction with conventional ZAF matrix corrections.

2.2. ^{27}Al MAS NMR. ^{27}Al MAS NMR spectra were collected for all of the YA glasses at 9.4 T and for selected compositions at 16.4 T. The high-field (16.4 T) spectra were obtained with single-pulse excitation on a Bruker Avance spectrometer operating at $\nu_o = 182.4$ MHz. Coarsely crushed glass samples were spun at 32 kHz in 2.5 mm (outside diameter) zirconia rotors. The spectra were acquired with 0.5 μs excitation pulse ($\nu_{RF} =$ 42 kHz), 0.2 s relaxation delay, 2000−8000 acquisitions, and 1 MHz digitization rate. The time-domain data were shifted to the origin and the first 8 μs recalculated by linear-prediction methods to reduce baseline and frequency-dependent phase errors. A short relaxation time was used to reduce intensity from crystalline phases, the resonances from which exhibit much longer spin−lattice relaxation times than those from the glass phases. We observed no change in the relative intensities for peaks from glass upon varying the relaxation delay from 0.1 to 5 s.

Spectra for all samples were collected with a Chemagnetics CMX-400 spectrometer operating at 104.3 MHz. Glass samples (ca. 60 mg) were spun at 15−16 kHz in zirconia rotors with an OD of 4 mm. For both spectrometers, the position of the sample probe assembly was adjusted to remove a background signal from the electronic components. Chemical shifts for ^{27}Al for both the low- and high-field spectra are reported relative to an external sample containing $Al(H_2O)_6^{3+}$ in the form of an acidic aqueous solution 0.1 M in $Al(NO_3)_3$.

An ^{27}Al triple quantum−single quantum MAS (3QMAS) experiment was performed for the two-phase glass, Y62.5A, at 16.4 T and 30 kHz spinning rate. A zero-quantum filtered pulse sequence was used with pulses of 2.2 and 0.8 μs at $\nu_{RF} \approx 150$ kHz, followed by a selective $\pi/2$ pulse of 12.5 μs. We collected 128 t_1 slices in increments of 16.67 μs, each corresponding to 240 transients at a recycle delay of 2 s.

2.3. Calorimetry. Differential scanning calorimetry was performed on ~200 mg batches of coarsely crushed glass in the temperature range 300−1000 K with a Setaram DSC-111 and on ~50 mg batches of coarsely crushed glass at 300−1725 K with a Netzsch DSC-404. Heat capacities of the glasses and supercooled liquids were obtained using standard calorimetric procedures.[16] Continuous scans of the baseline, standard, and sample were performed, at scanning rates of 10 K/min with the DSC-111 and 20 K/min with the DSC-404. Baseline corrections were applied to both the standard and sample runs. Calibrations of the Setaram and Netzsch instruments were obtained using high purity α-Al_2O_3 before and after completing the calorimetric measurements. The calibration curves were obtained by using measured values of the alumina standard in conjunction with accepted values for the heat capacity of α-Al_2O_3.[17]

The heat capacity of the glass was measured quantitatively as a function of temperature with the Setaram instrument. Repeated scans on each glass sample, i.e., successive cycling from 300 to 1000 K, allowed relaxation of the glass to occur. These data obtained on the glasses using the Setaram instrument were used as calibration curves for data obtained using the Netzsch instrument, which accessed higher temperatures. Glasses analyzed using the Netzsch instrument were as-made, i.e., unrelaxed; however, when calibrated with the quantitative C_P vs T curves for the glass, it was possible to quantify the change in heat capacity at T_g and values of C_P for the supercooled liquid. It is noted that the glass transition and crystallization temperatures are for scans performed at 20 K/min.

3. Results

3.1. Glass Synthesis. Results from the glass synthesis experiments are given in Table 1. The sample identification number refers to the nominal aluminum oxide content in mole %. The analyzed mole % Al_2O_3 (balance Y_2O_3) ranges from 59.79 to 75.63 mol %, as calculated from the average measured compositions in weight % oxide. The measurement errors shown in parentheses are one standard deviation of the mean value derived from 15 to 20 analyses per sample.

The glass ([g1], [g2]), and crystalline, ([x]) phases observed in the samples are reported in Table 1. The bulk of all samples was glass, [g1]. The second glass phase, [g2], formed as spheroids in a matrix of [g1] for lower alumina compositions (60−69 mol % alumina). The spheroid phase was readily observed in the two-phase glasses with an optical microscope, and was estimated to be 15 to 20 volume % of the glass for samples with the lowest alumina contents. This proportion decreased with increasing alumina, until, at the Y69A composition, the spheroid phase was observed only in the samples with the lowest cooling rates, i.e., the largest samples. Backscattered electron imaging was also used to examine the two glass phases, and the BSE images showed no evidence for the spheroid phase in samples with alumina contents at or above 69 mol %. BSE imaging also showed that, for the Y62.5A composition, the cathodoluminescence of the glass matrix was very weak (light blue), whereas that of the spheroid phase was very strong (bright blue). This feature, which was also reported by Weber et al.,[5] suggests the spheroid and matrix phase differ in density and that the spheroid phase may contain at least some crystalline material. This interpretation is consistent with the results of Nagashio and Kuribayashi[14] and with the NMR results from this study, as discussed below. Within two sigma measurement errors, the spheroid and matrix glass phases of sample Y65A are compositionally identical (Table 1), consistent with results of earlier work.[2,5]

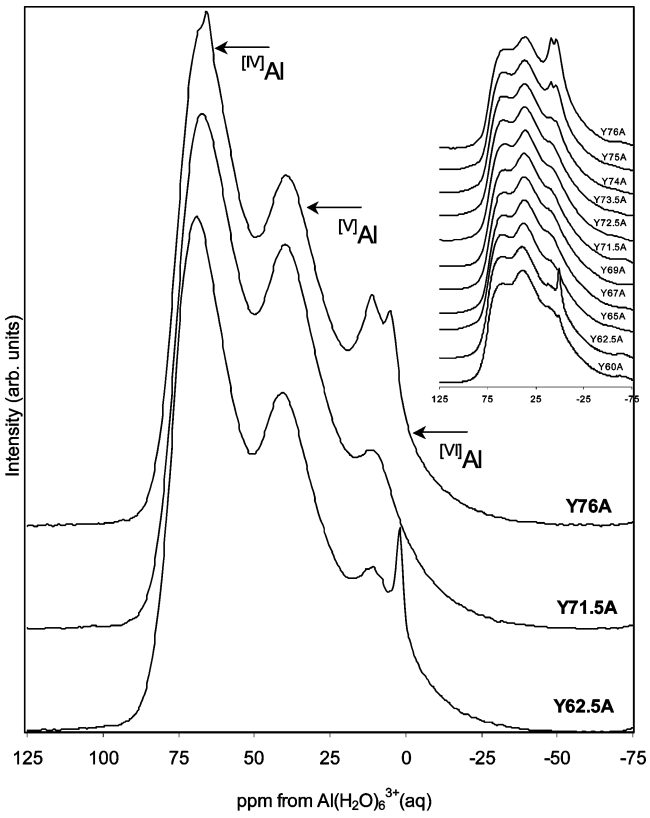

Figure 1. ^{27}Al MAS NMR spectra for the two-phase Al_2O_3−Y_2O_3 glasses, Y62.5A and Y76A, and the single-phase glass, Y71.5A, taken at 182.4 MHz (16.4 T). Resonances in the 65, 40, and 10 ppm regions represent Al^{3+} in 4-, 5-, and 6-coordination, respectively. Data represent 6000 transients obtained by single-pulse excitation (0.5 μs), with 0.2 s relaxation delay and 32 kHz spinning rate. Inset shows 104.3 MHz (9.4 T) spectra for all glasses in the compositional suite.

Single-phase glasses with no spheroid phase and no evidence of crystalline material were obtained in the composition range from Y69A to Y73.5A. Single-phase glasses containing minor amounts of crystalline material were formed from compositions with 73.5 to 76 mol % alumina. Larger specimens formed from the Y73.5A composition displayed a thin crystalline coating around the single-phase glass core material; this coating became thicker, and more differentiated, with increasing alumina.

The lowest values of cooling rates at which glass was formed for each composition approximate the critical cooling rates, R_C, and range from 50 to 230 K/s. The crystal nucleation temperature (T_N) for liquids cooled at rates less than R_C was insensitive to composition, giving $T_N \approx 1300$ K, the temperature at which the cooling rates were recorded.

3.2. ^{27}Al MAS NMR Spectra. *3.2.1. High-Field Spectra.* The ^{27}Al MAS NMR spectra taken at 16.4 T for Y62.5A, Y71.5A, and Y76A glasses are shown in Figure 1. Three broad, asymmetrical peaks with maxima near 67, 40, and 10.5 ppm are assigned to Al^{3+} ions in 4-, 5-, and 6 -coordination to oxygen, respectively. Two samples show minor peaks due to crystalline phases, at 1.4 ppm in Y62.5A and 3.9, 10.1, and 65 ppm in Y76A. Comparison with the results of Florian et al.[6] suggests that the peak at 1.4 ppm is due to the presence of YAG crystals in Y62.5A and the peak at 10.1 ppm is due to $YAlO_3$−perovskite crystals in Y76A. The other peaks cannot be assigned to known crystalline phases at this time.

The relative populations of Al^{3+} coordination environments were obtained from the ratios of the main peaks by fitting the

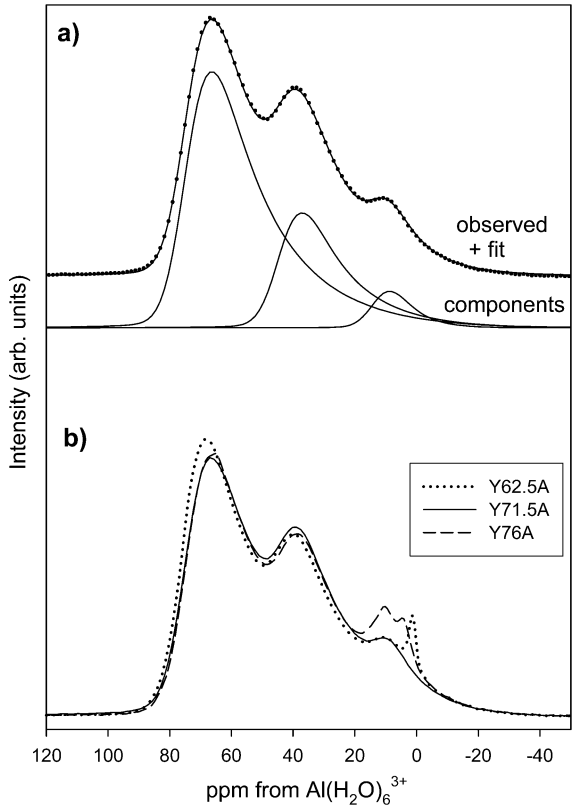

Figure 2. (a) ^{27}Al MAS NMR spectrum (182.4 MHz) for Y71.5A glass and a fitted profile calculated assuming a distribution of EFG's, giving the values listed in Table 2. Similar parameters also fit well the glass component for spectra of Y76A and Y62.5A. Dots are observed data and the upper trace is the fitted profile, which is the sum of the lower traces due to $^{[IV]}$Al, $^{[V]}$Al, and $^{[VI]}$Al components, vertically offset for clarity. (b) ^{27}Al MAS NMR spectra taken at 182.4 MHz, plotted with intensities normalized according to glass content. Peaks for crystalline phases in Y62.5A (including unresolved $^{[IV]}$Al from YAG) and Y76A were fit with Gaussian curves and their intensities subtracted from the total. Glass components were approximated by line shapes similar to those in a. Adjustments for central transition and satellite spinning sidebands were insignificant under these conditions.

TABLE 2: Results of High-Field ^{27}Al MAS NMR Analyses on Yttria−Alumina Glasses

property	glass	$^{[4]}$Al	$^{[5]}$Al	$^{[6]}$Al
relative intensity	Y76A	67.5	24.5	7.8
	Y71.5A	67.7	26.8	5.5
	Y62.5A	69.0	24.3	6.7
ave. chemical shift	Y71.5A	75.1	44.8	13.3
ave. QCC (MHz)	Y71.5A	9.5	8.6	5.8
QCC distribution (1σ)	Y71.5A	4.2	3.8	2.6

1-d spectra to a sum of components corresponding to distributions of electric field gradients (EFGs) plus Gaussian curves to account for crystalline components. EFG distributions and the resulting values of nuclear quadrupole coupling constant (C_Q) and asymmetry parameter (η) were calculated according to the method described by Coster et al.[18] Spectral profiles were calculated by summation of the scaled second-order quadrupolar MAS powder patterns, and compared to the observed spectra, using a simplex algorithm to search parameter space for minimum residuals.

The result for the single-phase sample Y71.5A is shown in Figure 2, with the best-fit parameters given in Table 2. The fit is not a unique solution, but similar parameter sets provide good fits to the spectra of all three samples. Large average C_Q values with significant distributions were required to fit the centerband

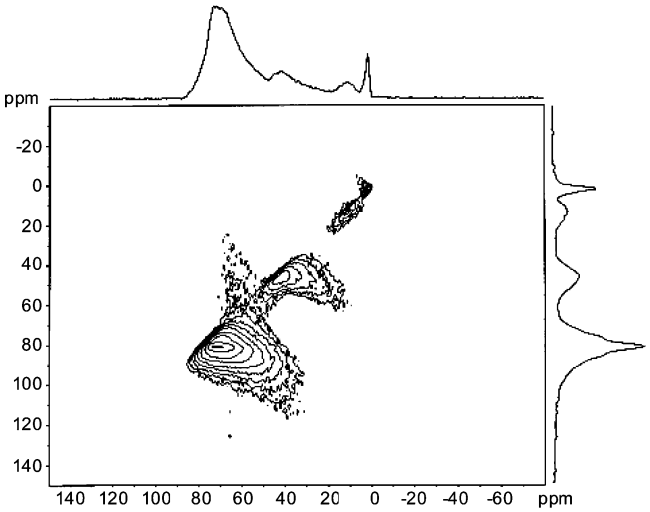

Figure 3. Sheared 3Q-MAS spectrum for Y62.5A (YAG-composition) glass with the isotropic projection (F1) on the right and anisotropic projection (F2) at the top. Contours are drawn at 7, 10, 15, 18, 26, 38, 56, 82, and 99% of maximum intensity. The F1 frequencies are scaled by a factor of 12/31 (ref 20). Spectrum was obtained at 182.44 MHz on a Bruker Avance-700 spectrometer ($128t_1$ increments at 16.67 μs, 30 kHz spinning frequency).

profiles. Random distributions of EFGs yield distributions of C_Q values that are approximately Gaussian, characterized by the average C_Q and 1σ widths listed in Table 2. This line shape simulation method assumes that distributions of chemical shift (δ_i) and C_Q are not correlated. However, the MQ-MAS data (see below) suggest that this assumption is not entirely justified. For this reason, we use these simulations only as approximate line shapes for purposes of determining populations and place no physical significance to the other fitted values.

This analysis of the Y71.5A spectrum yields 68 ± 4%, 27 ± 3%, and 6 ± 2% for 4-, 5-, and 6-coordinated Al^{3+}, respectively, for the glass phase(s). The estimated uncertainties span the values obtained with small variations in the average value and distribution of the other line shape parameters. Using similar distributions of EFGs to analyze the Y62.5A and Y76A spectra fits the relative intensities within the estimated uncertainty (Table 2). Normalizing the spectral intensities by subtracting out the fitted intensity attributed to crystalline phases indicates that the $^{[5]}$Al intensity is probably slightly higher for Y71.5A than for Y76A and Y62.5A (Figure 2b).

3.2.2. Low-Field Spectra. Spectra taken at 9.4 T for the entire eleven-sample compositional suite are shown in the Figure 1 inset. Resolution is decreased relative to the 16.4 T data by quadrupolar broadening effects. Furthermore, a significant fraction of the intensity for all samples occurs as a broad, unresolved component that spans +300 to −200 ppm. This unresolved component is likely due to Al sites that experience very large EFGs. Quantitative information about the distribution of Al among coordination environments cannot be accurately determined from these low-field single-pulse spectra. The results do, however, qualitatively illustrate general trends in the NMR data. For example, glasses containing 64.5 to 73.1 mol % alumina (i.e., Y65A to Y73.5A) show no evidence of the sharp peaks due to crystalline phases that are present in the spectra for samples with the highest and lowest alumina contents.

3.2.3. 3QMAS. The 3QMAS spectrum for Y62.5A is shown in Figure 3. The horizontal (F2) axis corresponds to the anisotropic MAS dimension (δ_2), whereas the vertical (F1) axis is the isotropic dimension, which lacks broadening due to orientation-dependent shifts. Peaks in the isotropic dimension

occur at a position (δ_1) determined by a sum of the chemical shift (δ_i) and an isotropic quadrupolar shift[19]

$$\delta_1 = \delta_i + \delta_{QS} \quad (1)$$

$$\delta_{QS}(\text{ppm}) = \frac{3 \times 10^6}{850} \frac{Cq}{\nu_0^2}\left(1 + \frac{\eta^2}{3}\right)^2 \quad (2)$$

Projection in the isotropic dimension reveals broad peaks centered near δ_1 values 14, 47, and 82 ppm from the glass phases plus narrow peaks at $\delta_1 = +2.1$ ppm and $+81$ ppm (the latter superimposed on the broad peak). The positions of the narrow peaks agree nearly exactly with those expected for crystalline YAG based on the results of Florian et al.:[6] $\delta_i = 2.1$ ppm, $C_Q \approx 0$ for $^{[VI]}$Al; $\delta_i = 77.5$ ppm, $C_Q = 6.2$ MHz for $^{[IV]}$Al. The relative intensities of these crystalline YAG peaks are greater in the 3QMAS spectra than in the single-pulse spectrum (Figure 1), partly because a longer relaxation delay was used.

Some additional information about the distribution of Al environments can be inferred from comparison of the 3QMAS F1 and F2 dimensions (Figure 3) and the 1-D single-pulse MAS spectrum (Figure 1). For the $^{[VI]}$Al peak, almost all of the intensity lies along the $\delta_1 = \delta_2$ line, which suggests that most of the octahedral Al experience a small quadrupole interaction and that the width of this peak in the F1 dimension (11 ppm, fwhm) results primarily from a distribution of chemical shifts. Based on this information, we re-fit the 1-D MAS spectra with Gaussian-shaped peaks for the $^{[VI]}$Al, which yielded smaller average chemical shifts (11.3 ppm) but relative intensities similar to those displayed in Table 2.

Peaks for both $^{[IV]}$Al and $^{[V]}$Al in the glass phases show significant off-axis intensity indicating the presence of Al sites with large quadrupolar interactions. Comparison of the F2 3QMAS projection (Figure 3, top) with the 1D-MAS spectrum for Y62.5A in Figure 1, however, shows that the peaks in the 3QMAS spectrum are significantly more narrow, consistent with nonuniform excitation biased against sites with large C_Q values.[20] This observation is also reflected in the relative intensities of the glass peaks in the isotropic 3QMAS projection (66.9%, 22.5%, and 10.6% for 4-, 5-, and 6-coordinated Al, respectively), which show significantly more signal from $^{[VI]}$Al than inferred from the 1-D MAS spectra (Table 2), because of the smaller quadrupolar interactions for these sites. The C_Q distribution for $^{[IV]}$Al obtained from fits to the 1-D data yield $\langle\delta_i\rangle = 76.5$ ppm and a peak in the δ_{QS} distribution near 6 ppm, the sum of which is similar to the observed 3QMAS δ_1 (82 ppm). However, the EFG distribution used to fit the 1-D MAS spectra yields more intensity in a broad tail toward more positive δ_1 values than observed in the 3QMAS projection. The contour map also suggests some correlation between δ_i and C_Q values for $^{[IV]}$Al and $^{[V]}$Al sites. For example, the anisotropic (horizontal) line width for $^{[V]}$Al with δ_i near $+35$ ppm appears significantly smaller than for those with δ_i near $+45$ ppm, indicating smaller average C_Q for sites with smaller chemical shifts.

In contrast to the results of Florian et al.[6] for a sample of nearly identical composition, we observe only a single 3QMAS peak for $^{[V]}$Al in Y62.5A. This result suggests the possibility of structural differences arising from sample preparation.

3.3. Heat Capacity of the Glasses. A representative set of C_P vs T results obtained using the Setaram instrument are shown in Figure 4a for Y74A. As seen in the figure, the data are for the glass phase only, as the upper temperature limit was below T_g. Similar C_P vs T data sets were obtained for each for each of

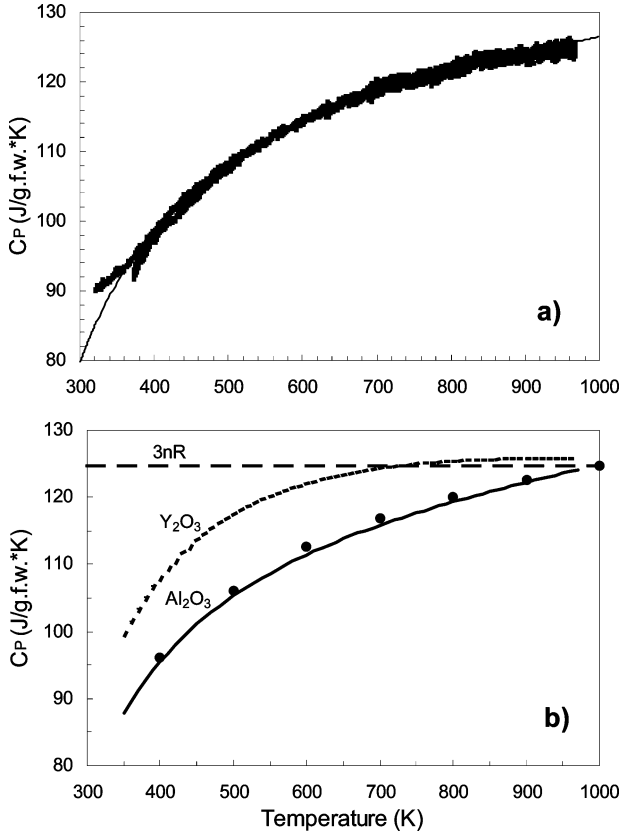

Figure 4. (a) Representative set of C_P results for Y74A glass, obtained using a Setaram DSC-111. A Maier-Kelley equation of the form $C_P = a + bT + cT^{-2}$ was fitted through the six measured C_P data sets for Y74A and the solid line represents the curve fit. Coefficients of the equation and associated errors for Maier-Kelley curve fits for each sample data set are reported in Table 3. (b) Global fit of heat capacity data for all sample glasses. The solid and dotted lines are the derived molar C_P results for Al_2O_3 and Y_2O_3, respectively. The dashed line marks the Dulong-Petit value (3nR). The solid circles are literature values for α-Al_2O_3.[25]

the eleven glasses in the YA system. The results were reproduced within $\pm 1\%$ on duplicate samples and are described to within $\pm 1\%$ between 350 and 975 K by the Maier-Kelley[21] equation

$$C_P = a + bT + cT^{-2} \quad (3)$$

The regression constants, a, b, and c for each composition are shown in Table 3.

A global fit of the data for all compositions is shown in Figure 4b and was obtained under the assumption that partial molar heat capacities are independent of composition. The Maier-Kelley equation was used to represent the partial molar values

$$\bar{C}_{P,i} = \bar{a}_i + \bar{b}_i T + \bar{c}_i T^{-2} \quad (4)$$

with components, i, taken as Al_2O_3 and Y_2O_3. The heat capacity results for all compositions were then fitted to the equation

$$C_P = \sum X_i \bar{a}_i + T \sum X_i \bar{b}_i + T^{-2} \sum X_i \bar{c}_i \quad (5)$$

where $\bar{C}_{P,i}$ is the partial molar heat capacity of component i; a_i, b_i, and c_i are the coefficients; T is the absolute temperature; C_P is the total molar heat capacity for the two-component system; and X_i is the mole fraction of component i. The global fit reproduced the values derived from the fits for each composition with an rms deviation of 0.88%. The coefficients, a_i, b_i, and c_i,

TABLE 3: Parameters of the Maier-Kelly Equation ($C_P = a + bT + cT^2$) for Yttria−Alumina Glasses

sample	scans	a	S.E. coeff (% of a)	$b \times 10^2$	S.E. coeff (% of b)	$c \times 10^{-5}$	S.E. coeff (% of c)	T range (K)
Y76A	3	116.600	0.22	1.3395	2.2	−36.72119	0.72	320−965
Y75A	3	124.286	0.19	0.3397	5.9	−44.50873	0.60	370−965
Y74A	6	115.367	0.15	1.4755	1.4	−35.92201	0.51	320−965
Y73.5A	3	122.805	0.20	0.6280	4.8	−42.97033	0.59	320−965
Y72.5A	6	116.584	0.16	1.3045	1.5	−36.38600	0.53	320−965
Y71.5A	3	121.641	0.17	0.5783	3.5	−42.25031	0.54	370−965
Y69A	3	114.615	0.16	1.6371	1.2	−31.96001	0.54	320−965
Y67A	3	117.675	0.16	0.9962	2.0	−33.20748	0.52	320−965
Y65A	3	128.889	0.18	−0.1833	10.9	−45.95176	0.55	370−965
Y62.5A	3	128.671	0.17	−0.1108	18.0	−46.64444	0.54	370−965
Y60A	3	117.693	0.20	1.4358	1.4	−36.47986	0.72	370−965
partial molar values:								
Al_2O_3		110.9	4.9	1.749	64	−35.84	15	
Y_2O_3		142.1	2.8	−1.172	19	−47.38	9.0	

TABLE 4: Results of Differential Scanning Calorimetry for Yttria−Alumina Glasses

	glass transition characteristics				supercooled liquid interval						
sample	T_g onset (K)	T_g peak (K)	$\Delta C_P(T_g)$ (J/gfw·K)[a]	T_g width (K)	T^{init} (K)	T^{final} (K)	ΔSCL T (K)	C_P^{init} (J/gfw·K)	C_P^{final} (J/gfw·K)	Δ SCL C_P (J/gfw·K)	T_x onset (K)
Y76A	1156	1183	53.15	31	1187	1198	11	183.66	168.93	14.73	1214
Y75A	1154	1182	66.16	31	1185	1199	14	192.20	175.06	17.14	1215
Y74A	1150	1181	73.35	34	1184	1200	16	200.02	180.39	19.63	1216
Y73.5A	1153	1179	79.99	31	1184	1200	16	205.34	184.10	21.24	1217
Y72.5A	1151	1178	74.44	32	1183	1203	20	204.24	182.43	21.81	1224
Y71.5A	1151	1179	78.73	31	1182	1205	23	203.63	182.24	21.39	1224
Y69A	1148	1178	71.96	31	1179	1204	25	206.42	185.89	20.53	1219
Y67A	1147	1176	79.73	31	1178	1195	17	207.46	190.41	17.05	1208
Y65A	1149	1175	80.16	29	1178	1191	13	205.35	184.47	20.88	1202
Y62.5A	1147	1173	44.09	26	1173	1173	<1	171.48	170.17	1.31	1196
Y60A	1146	1172	61.04	27	1173	1173	<1	194.18	192.57	1.61	1195

[a] gfw $= \Sigma\, MW_i * X_i$, $i = Al_2O_3$ and Y_2O_3.

derived from the global fit are included in Table 3. The presence of a small amount of crystalline material in glasses near the composition limits for glass formation does not influence these results, since the heat capacities of glasses and the corresponding crystalline materials are nearly identical.

3.4. Heat Capacity Changes at T_g. Fitted C_P vs T curves for the glasses along with data to higher temperatures obtained with the Netzsch instrument are shown in Figure 5 for the same three compositions (Y76A, Y71.5A, and Y62.5A) for which NMR results are given in Figure 1. Results derived from the measurements are reported in Table 4 for all eleven compositions. Determination of the properties listed in Table 4 is illustrated schematically in Figure 5 for Y71.5A. The Netzsch DSC measurements were performed on the as-made glasses, so the results exhibit glass relaxation below T_g, manifested as a broad and weak exotherm in the temperature range from 1050 to 1150 K and a minimal overshoot in the C_P values at the glass transition.

The glass transition temperature is nearly independent of composition, showing only a slight increase, from 1146 to 1156 K, with increasing alumina content. We obtain $\Delta C_P(T_g) = 76.9 \pm 3.5$ J/gfw·K as the average heat capacity difference between the glass (at T_g onset) and supercooled liquid (at T^{init}) for seven glasses in the YA compositional suite. Results for four compositions, two at each end of the composition range, were not used in calculating this average value. The samples not included exhibited substantially smaller $\Delta C_P(T_g)$ values, perhaps due to the presence of crystalline material in the high-alumina compositions and both crystalline material and a second glass phase in the low-alumina compositions. BSE imaging of the cross section for a Y76A sample showed a crystalline layer of ∼40 μm thickness on a 1.3 mm diameter sample. The glass material thus represents ∼83% of the sample volume which is sufficient to explain the reduced $\Delta C_P(T_g)$ value. The width of the T_g range is relatively insensitive to composition, ranging from 26 to 34 K.

3.5. Heat Capacity of the Supercooled Liquid. Initial and final temperatures and heat capacities for the supercooled liquid (SCL) interval are given for all compositions in Table 4. Values for the heat capacities of the supercooled liquids at the low temperature end of the SCL interval range from 200 to 207 J/gfw·K (Table 4) for samples containing 65−74 mol % alumina, the same compositional set for which an average value of $\Delta C_P(T_g)$ of 76.9 ± 3.5 J/gfw·K is obtained (see section 3.4).

Figure 5 shows a small SCL temperature interval above T_g for samples Y76A and Y71.5A. In this region, the C_P values show a rapid and linear decrease with temperature up to the onset of exothermic transitions. Indeed, for all of the samples except Y60A and Y62.5A, the heat capacity of the supercooled liquid decreases by approximately 20 J/gfw·K over an ∼20 K temperature interval above the T_g peak. This small SCL interval renders it difficult to separate the effects of the onset of higher temperature exotherms from a negative temperature dependence to the C_P of the SCL. For samples Y62.5A (e.g., Figure 5) and Y60A, no supercooled liquid range is discernible on the C_P vs T curves; the glass transition appears to be truncated by crystallization.

4. Discussion

4.1. Phase Formation and Structure of Glasses in the YA System. The present work demonstrates single-phase YA glass formation over the composition range from 69.0 to 75.6 mol % aluminum oxide and supports the conclusion that polyamorphism occurs in YA glasses with alumina concentrations lower than ∼69 mol %. These results show that our earlier conclusion[5]

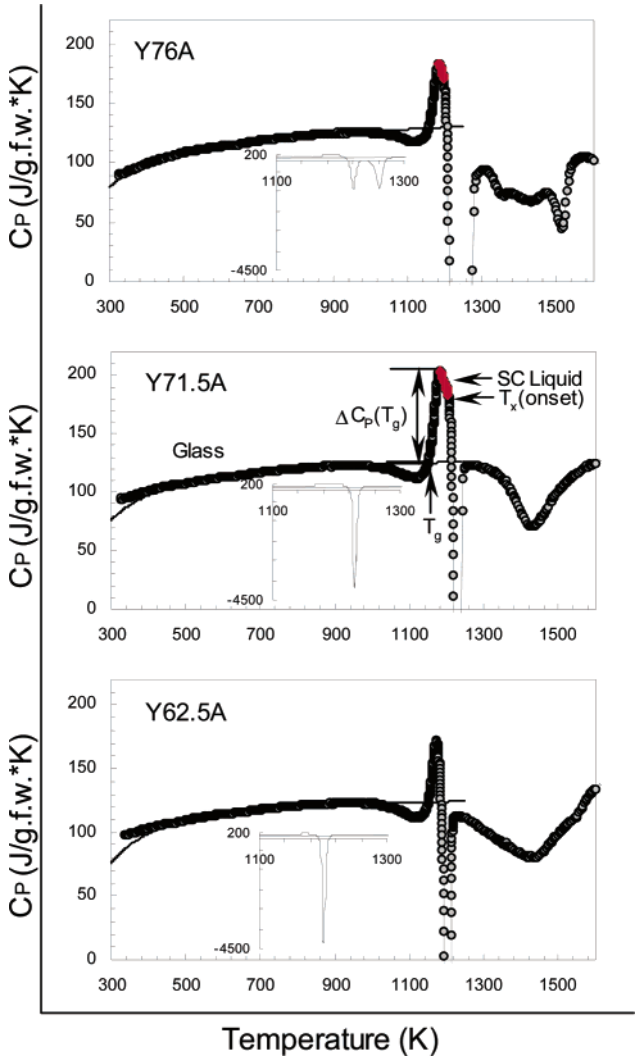

Figure 5. Heat capacity data for a representative set of YA glasses. The solid lines represent Maier-Kelley curves, which were fitted through the C_P data for the glass, as in Figure 4a. C_P data through the glass, the glass transition region, and the supercooled liquid interval, shown as solid circles, were obtained using the Netzsch DSC-404 and have been calibrated with the fitted curves obtained using the Setaram DSC-111. As illustrated for Y71.5A, glass transition temperatures, T_g, are taken at the transition onsets where the extrapolated fitted C_P curves for the glasses intersect the rise in C_P through the glass transition. Values for the increase in heat capacity at the glass transition, $\Delta C_P(T_g)$, were obtained by subtracting the values for the C_P of the fitted glass at T_g from the lowest temperature values for the C_P of the supercooled liquids. The T_g width was determined as the difference in temperature between the onset and end of the glass transition, where the T_g end is equal to the beginning of the SCL regime. The supercooled liquid interval is marked by the red circles superimposed on the dark circles at $T > T_g$ for samples Y76A and Y71.5A. Y62.5A had no discernible supercooled liquid phase. T_x marks the onset of exothermic phase transitions and is also equal to the end of the SCL regime. Insets show the exothermic transitions which occur at temperatures beyond the SCL regime.

that two-phase YA glasses can be prepared over the entire composition range from 58 to 77 mol % Al_2O_3 requires correction. Our earlier report was based on results for glass compositions with 76.9, 68.8, and lower mole percentages of alumina. Samples with $Al_2O_3 \leq 68.8$ are outside the composition range for single-phase glass. The glass with 76.9 mol % alumina is in the range for single-phase glass formation but appeared cloudy. As demonstrated in this work, a cloudy appearance is not a definitive indicator of two-phase glasses, since it can also result from the thin crystalline layer that forms on the glasses with higher alumina compositions. We cannot confirm the reappearance of two-phase glasses at even higher alumina contents that is reported by Wilding and McMillan;[9] cooling rates sufficient to obtain glass with more than 76 mol % alumina were not achieved in the current work.

The observation of both single and two-phase glass at the Y69A composition indicates that a critical cooling rate is required, not only for glass formation, but also for two-phase glass formation, i.e., polyamorphism. We anticipate that polyamorphic glasses may also be formed for compositions where single-phase glasses were obtained in this work, by using slower cooling rates or perhaps by heating into the supercooled liquid range. Investigations to explore these possibilities are currently underway.

The variations in 4-, 5-, and 6-coordinate Al concentrations among glass compositions (see Table 2) are small, but the relative changes are likely determined with a greater precision than the ±4, ±4, and ±3% estimated uncertainty for the accuracy of their respective values. Assuming that the distributions of C_Q and δ_i do not vary significantly among these samples, then the variations in relative intensity for each type of site reflects changes in the spectral profiles. This effect can be clearly seen for $^{[V]}$Al when the spectra are normalized to equal area for the glass component (Figure 2b). If the trends in species concentration are correct, a minimum in the 6- and a maximum in the 5-coordinate Al concentration occurs near the Y71.5A composition. We suggest that the reversal in these trends with composition may be explained by the appearance of polyamorphism at alumina contents less than the Y69A composition. If this line of reasoning is valid, the polyamorphic spheroid glass phase will have decreased 5- and increased 6-coordinate Al concentrations relative to the matrix glass in which it forms.

It should be noted that all NMR experiments were performed on the as-synthesized, i.e., unannealed, YA glasses. Previous studies[22,23] show that the proportion of higher coordinate Al (particularly $^{[V]}$Al) species in aluminate and aluminosilicate glasses is higher in fast-quenched relative to slowly cooled glasses, and that annealing can reduce the proportion of higher coordinate Al^{3+} in favor of $^{[IV]}$Al. Containerless processing may also have an effect on the relative proportions of $^{[IV]}$Al, $^{[V]}$Al, and $^{[VI]}$Al, though this is untested. Further studies are underway to investigate the structural effects of annealing and post-T_g thermal treatment of the YA glasses.

4.2. Nature of Polyamorphism in YA Liquids. Although polyamorphism has been viewed as a newly described class of phenomena,[2,24] an alternative explanation is that it results from a kinetically modified first-order phase transition between two dense fluids. Figure 6 shows a temperature−composition phase diagram for a classical fluid−fluid phase transition in a two-component system that illustrates this idea. Each pure component exhibits a congruent transition between the two liquids, chosen at 1600 and 1400 K in this example. Each liquid spans the composition range of the two-component system. Within this range, the two liquids can be at equilibrium only if their compositions differ or if the system exhibits an azeotrope, as shown by the minimum transition temperature in the figure.

Now consider a cooling experiment, represented by the arrow. Significant undercooling of the higher-temperature liquid is required to nucleate the second liquid phase at T_N. Congruent liquid−liquid transition is possible at any composition because nucleation and growth occur at a temperature where the stable lower-temperature liquid has a composition identical to that of the unstable higher-temperature liquid. This mechanism is

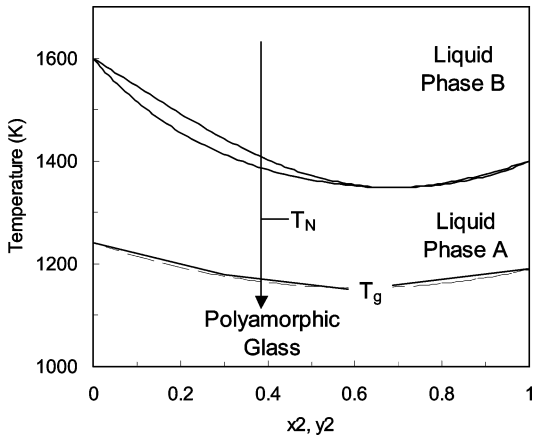

Figure 6. Phase diagram illustrating polyamorphism resulting from nucleation and incomplete growth of a second liquid phase prior to glass formation under rapid cooling conditions. The diagram is calculated assuming liquid−liquid transition enthalpies equal to 18 and 16 kJ/mol for pure components 1 and 2, respectively. Liquid-phase A is an ideal solution, and liquid-phase B is a symmetrical regular solution with an energy parameter, 6 kJ/mol.

entirely consistent with the observations of polyamorphism in the YA system where polyamorphic glass is obtained at relatively high cooling rates that quench the phase transition before it is complete. Two glasses, in the form of spheroids of the glass formed from the lower temperature liquid in a matrix glass formed from the higher temperature liquid, are the expected products.

The devitrification enthalpy of YAG-composition glass is 36 kJ/gfw smaller than the heat of fusion, which is a large enthalpy difference compared with the reaction enthalpy of only 18.8 kJ/gfw between α- and γ-Al_2O_3.[25] Thus, although α-Al_2O_3 is more stable than γ-Al_2O_3 at all temperatures, γ-Al_2O_3 becomes stable relative to the liquid at an undercooling of only ~50 K, and it is reasonable to propose that more than one liquid phase may also be stable over the large undercooled temperature range of YA melts. Thus, the phase diagram given in Figure 6 was calculated assuming transition enthalpies comparable to the enthalpy of reaction between α- and γ-Al_2O_3.

4.3. Thermodynamics of YA Glasses and Liquids. *4.3.1. C_P of Glasses.* Derived $\bar{C}_{P,i}$ values, as calculated from the coefficients reported in Table 3, are shown as a function of temperature in Figure 4b along with data from the literature. The figure shows that the derived partial molar C_P of Al_2O_3 in YA glasses is nearly equal to that of crystalline α-alumina;[25] the two values differ by less than 1% over the entire temperature range.

Thermodynamic models that accurately describe the heat capacity of multicomponent silicate glasses have been developed,[26,27] but these models do not apply to alumina-based or low-silica (<50 mol %) glasses. The inherent difficulty of glass formation in low-silica and alumina-based systems is a contributing factor to this scarcity of data. The heat capacity data reported herein on the YA glasses can ultimately be used in conjunction with additional C_P data on alumina-based glasses to derive partial molar heat capacities for oxides in multicomponent aluminate glasses, and in turn to develop models describing the C_P of alumina-based glasses.

4.3.2. Features of the Glass Transition. Liquids that exhibit large configurational heat capacity values ($\Delta C_P(T_g)$) are typically highly fragile.[24] Previous work indicates that liquids in the YA system with compositions at or near that of YAG are fragile.[5,7,11,12] Values of $\Delta C_P(T_g)$ determined in this study for the YA liquids (Table 4) provide an independent and quantitative measure of the relative fragility of these liquids. The values of $\Delta C_P(T_g)$ for the single-phase YA liquids are ~80 J/gfw·K (Table 4) and represent approximately 60% of the heat capacity of the glass at the glass transition temperature. By contrast, Richet and Bottinga[28] show that for molten silicates, the configurational component typically represents only about 10−30% of the heat capacity of the glass at T_g. In addition, values of $\Delta C_P(T_g)$ typically decrease with increasing T_g,[29] yet the YA glasses have high T_g values (~1150 K) and large configurational heat capacities. On a J/g·K basis, the $\Delta C_P(T_g)$ of the single-phase YA liquids (0.55−0.60 J/g·K) is essentially the same as the value obtained for CKN ($40Ca(NO_3)_2$:$60KNO_3$), 0.55 J/g·K.[30] CKN forms an ionic liquid and exhibits extremely fragile behavior.[24]

4.3.3. C_P of YA Liquids. The C_P of the supercooled YA liquid is significantly larger near the glass transition than averaged over the T_g-T_m range. For example, at the end of the SCL interval for sample Y69A, the sample which is predominantly single phase and closest in composition to YAG, the C_P is approximately 57 J/gfw·K greater than the extrapolated Maier-Kelley values for the glass. C_P values are approximately equal for a glass and the corresponding crystalline solids. Therefore, and for the YAG composition, we can infer that C_P(liquid) is approximately 57 J/gfw·K greater than C_P(YAG) at 1190 K, 43 K above the glass transition temperature. The average difference between C_p values for liquid and crystalline materials, ΔC_P(ls) over the entire supercooled liquid range can be calculated for the YAG composition from the equation

$$\Delta C_P(\text{ls}) = \frac{(\Delta H_{\text{devitrification}} + \Delta H_{\text{fusion}})}{(T_m - T_g)} \qquad (6)$$

Using T_g = 1150 K, T_m = 2240 K,[31] $\Delta H_{\text{devitrification}}$ = 69 kJ/gfw,[13] and ΔH_{fusion} = −105 kJ/gfw,[1] we obtain ΔC_P(ls) = 33 J/gfw·K, considerably smaller than the value near the glass transition. This result shows that a substantial further decrease in the liquid-crystal heat capacity difference for the YAG composition, and probably for all YA liquids, occurs as the liquid is heated from T_g to T_m.

5. Concluding Remarks: Relationship between Structural and Thermodynamic Properties

Different coordination values for Al^{3+} ions is a well-known feature of the different phases of Al_2O_3 and of the crystalline YA phases. For example, Al^{3+} occurs in both 4- and 6-coordination in γ-Al_2O_3 and $Y_3Al_5O_{12}$, is 6-coordinated in α-Al_2O_3 and $YAlO_3$, and is mostly 4-coordinated in Al_2O_3 liquid.[32] Although crystal energy would tend to be greater for the higher-coordinated environment, the Al−O bond length is also different, nominally 1.76 and 1.95Å, for 4- and 6-coordination, respectively. Thus, relatively small energy differences exist between 4- and 6-coordinated Al^{3+} ions, a feature that will influence the nature of polyamorphic aluminate glasses. The present NMR results support the idea that coordination changes also occur in the liquid−liquid-phase transition of YA melts, with increased 6- and decreased 5-coordinated species concentrations with conversion from the matrix to the spheroid phase.

The present research has provided quantitative thermodynamic and structural properties of YA glasses over the composition range from 59.8 to 75.6 mol % Al_2O_3. We report values for T_g, $\Delta C_p(T_g)$, concentrations of 4-, 5-, and 6-coordinated Al^{3+}, cooling rates for glass formation under containerless conditions, and the compositions at which polyamorphic glasses are

obtained. These results will be a useful guide for further experimental and theoretical investigations of polyamorphism. We believe that the polyamorphism observed in the YA system can be explained as a special case of conventional fluid−fluid phase transition and that the polyamorphic YA glasses that occur in this system will show significant differences in the concentrations of 5- and 6-coordinated Al.

Acknowledgment. This research was supported by NASA Physical Sciences Division under Grant No. NAS8-98092. The authors thank Dr. Sarah Roeske in the Department of Geology at the University of California−Davis for performing electron microprobe analyses, Juraj Majzlan in the Thermochemistry Facility at the UC−Davis for performing calorimetric scans on two of the samples, and Martine Ziliox for assistance with the high-field NMR measurements. Low-field NMR measurements were made at the W. M. Keck Solid-State NMR Laboratory at UC−Davis.

References and Notes

(1) Gervais, M.; LeFloch, S.; Rifflet, J. C.; Coutures, J.; Coutures, J. P. *J. Am. Ceram. Soc.* **1992**, *75*, 3166−68.
(2) Aasland, S.; McMillan, P. F. *Nature* **1994**, *369*, 633−36.
(3) Coutures, J. P.; Rifflet, J. C.; Billard, D.; Coutures, P. *Proc. 6th Eur. Symp. Mater. Sci. Under Microgravity Conditions*, Bordeaux, France; 1986; pp 427−30.
(4) Nagashio, K.; Takamura, Y.; Kuribayashi, K. *Mater. Sci. Forum* **2000**, *329*−*330*, 173−8.
(5) Weber, J. K. R.; Hixson, A. D.; Abadie, J. G.; Nordine, P. C.; Jerman, G. A. *J. Am. Ceram. Soc.* **2000**, *83*, 1868−72.
(6) Florian, P.; Gervais, M.; Douy, A.; Massiot, D.; Coutures, J.-P. *J. Phys. Chem. B* **2001**, *105*, 379−91.
(7) Wilding, M. C.; McMillan, P. F.; Navrotsky, A. *Physica A* **2002**, *314*, 379−90.
(8) Weber, J. K. R.; Krishnan, S.; Ansell, S.; Hixson, A. D.; Nordine, P. C. *Phys. Rev. Lett.* **2000**, *84*, 3622−26.
(9) Wilding, M. C.; McMillan, P. F. *J. Non-Cryst. Solids* **2001**, *293*−*295*, 357−65.
(10) Wilding, M. C.; Benmore, C. J.; McMillan, P. F. *J. Non-Cryst. Solids* **2002**, *297*, 143−55.
(11) Fratello, V. J.; Brandle, C. D. *J. Cryst. Growth* **1993**, *128*, 1006−10.
(12) Weber, J. K. R.; Felten, J. J.; Cho, B.; Nordine, P. C. *Nature* **1998**, *393*, 769−71.
(13) Lin, I.-C.; Navrotsky, A.; Weber, J. K. R.; Nordine, P. C. *J. Non-Cryst. Solids* **1999**, *243*, 273−76.
(14) Nagashio, K.; Kuribayashi, K. *J. Am Ceram. Soc.* **2002**, *85*, 2353−58.
(15) Weber, J. K. R.; Felten, J. J.; Nordine, P. C. *Rev. Sci. Instrum.* **1996**, *67*, 522−24.
(16) Mraw, S. C. In *Specific Heat of Solids, CINDAS Data Series on Material Properties*; Ho, C. Y., Ed.; Hemisphere Publishing Corporation: New York, 1988; Vols. 1−2, pp 395−437.
(17) Ditmars, D. A.; Douglas, T. B. *J. Res.* **1971**, *75A*, 401−20.
(18) Coster, D.; Blumenfeld, A. L.; Fripiat, J. J. *J. Phys. Chem.* **1994**, *98*, 6201−6211.
(19) Amoureux, J.-P.; Fernandez, C. *Solid State Nuclear Magn. Reson.* **1998**, *10*, 211−223.
(20) Ding, S.; McDowell, C. A. *Chem. Phys. Lett.* **1999**, *307*, 215−219.
(21) Maier, C. G.; Kelley, K. K. *J. Am. Chem. Soc.* **1932**, *54*, 3243−46.
(22) Poe, B. T.; McMillan, P. F.; Angell, C. A.; Sato, R. K. *Chem. Geol.* **1992**, *96*, 333−49.
(23) Sato, R. K.; McMillan, P. F.; Dennison, P.; Dupree, R. *J. Phys. Chem.* **1991**, *95*, 4483−89.
(24) Angell, C. A. *Science* **1995**, *267*, 1924−35.
(25) Chase, M. W., Jr.; Davies, C. A.; Downey, J. R., Jr.; Frurip, D. J.; McDonald, R. A.; Syverud, A. N. *JANAF Thermochemical Tables, Third Edition*; Physical and Chemical Reference Data, Am. Chem. Soc.; American Institute of Physics: New York, 1985.
(26) Stebbins, J. F.; Carmichael, I. S. E.; Moret, L. K. *Contrib. Mineral. Petrol.* **1984**, *86*, 131−48.
(27) Richet, P. *Chem. Geol.* **1987**, *62*, 111−24.
(28) Richet, P.; Bottinga, Y. *Geochim. Cosmochim. Acta* **1985**, *49*, 471−86.
(29) Hodge, I. M. *J. Non-Cryst. Solids* **1994**, *169*, 211−66.
(30) Hempel, E.; Hempel, G.; Hensel, A.; Schick, C.; Donth, E. *J. Phys. Chem. B* **2000**, *104*, 2460−66.
(31) Caslavsky, J. L.; Viechnicki, D. J. *J. Mater. Sci.* **1980**, *15*, 1709−18.
(32) Ansell, S.; Krishnan, S.; Weber, J. K. R.; Felten, J. J.; Nordine, P. C.; Beno, M. A.; Price, D. L.; Saboungi, M.-L. *Phys. Rev. Lett.* **1997**, *78*, 464−6.